Supplementary information

Non-competitive additives regulate molecular assembly for compact monolayers in perovskite/silicon tandems

Lirong Zeng,[1,5] Bingyu Qi,[2,5] Xin Zhang,[1,5] Xinjiang Wang,[2] Meng Wei,[1] Lijun Yang,[1] Naihe Liu,[1] Yuwei Geng,[1] Yan Liu,[1] Ying Zhu,[1] Cheng Zhu,[3] Qi Chen,[3] Guanjun Yang,[1] Kaifu Qiu,[4,*] Lijun Zhang,[2,*] and Bo Chen[1,*]

[1] State Key Laboratory for Mechanical Behavior of Materials, School of Materials Science and Engineering, Xi'an Jiaotong University, Xi'an, Shaanxi 710049, China.

[2] School of Materials Science and Engineering, Jilin University, Changchun, Jilin 130022, China.

[3] School of Materials Science and Engineering, Beijing Institute of Technology, Beijing 100081, China.

[4] Zhejiang Aiko Solar Energy Technology Co., Ltd., Jinhua, Zhejiang 321000, China.

[5] These authors contributed equally: Lirong Zeng, Bingyu Qi, Xin Zhang.

* e-mail: qiukaifu@aikosolar.com (K.Q.), lijun_zhang@jlu.edu.cn (L.Z.), bochen@xjtu.edu.cn (B.C.).

Contents

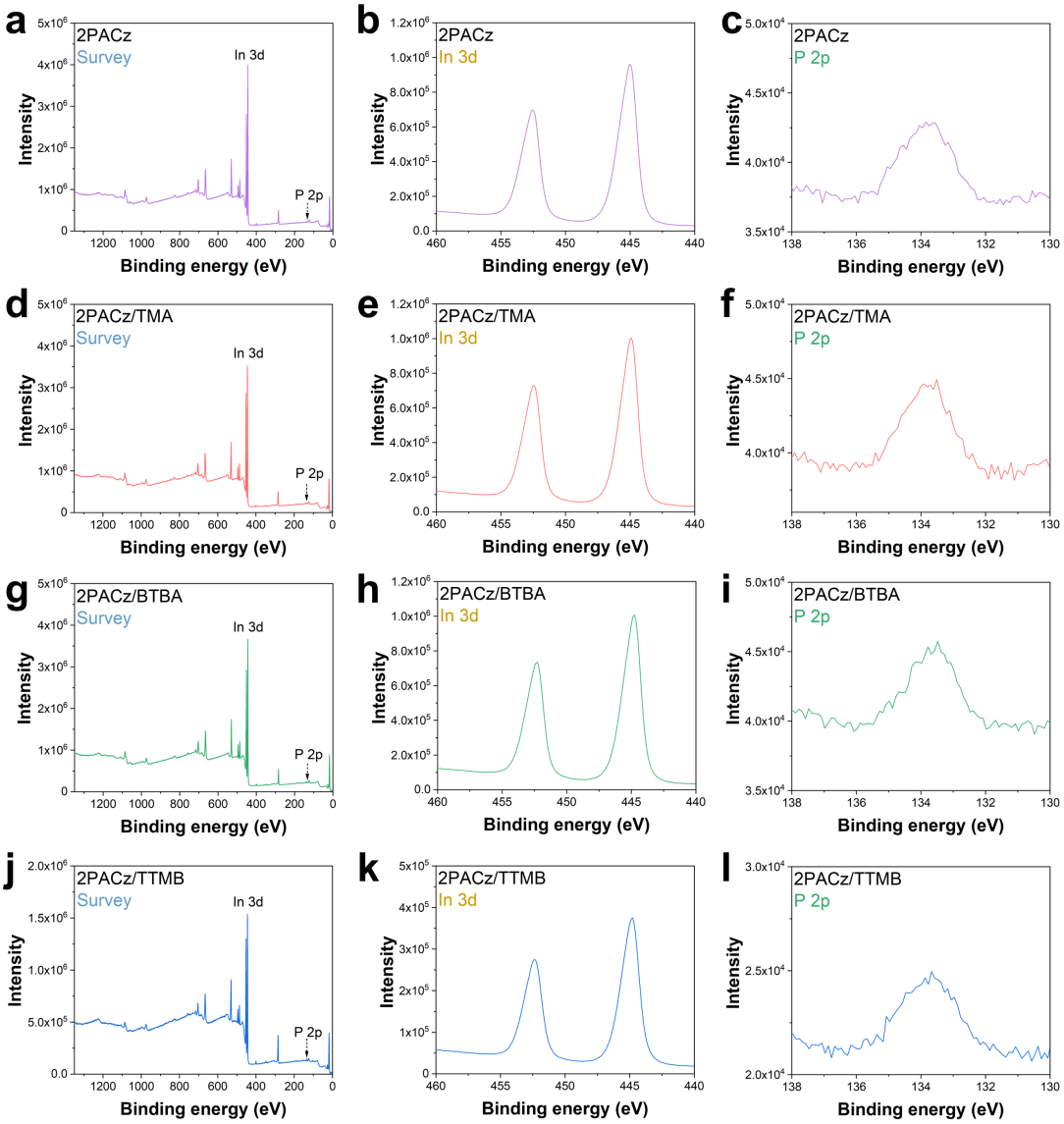

Supplementary Fig. 1. XPS spectra of SAM/ITO/glass samples prepared from 2PACz solutions with different additives. (**a-c**) pristine 2PACz without additive. (**d-f**) 2PACz with TMA. (**g-i**) 2PACz with BTBA; (**j-l**) 2PACz with TTMB. (**a, d, g, j**) XPS survey spectra. (**b, e, h, k**) In 3d XPS spectra. (**c, f, i, l**) P 2p XPS spectra.

The P/In atomic ratio, determined from the P 2p XPS signals of 2PACz and In 3d XPS signals of the ITO substrate, serves as an indicator of effective SAM surface density on ITO substrate. Higher P/In ratios correspond to increased 2PACz density on

the substrate. Analysis shows that the inclusion of additives enhances the P/In ratio relative to pristine 2PACz.

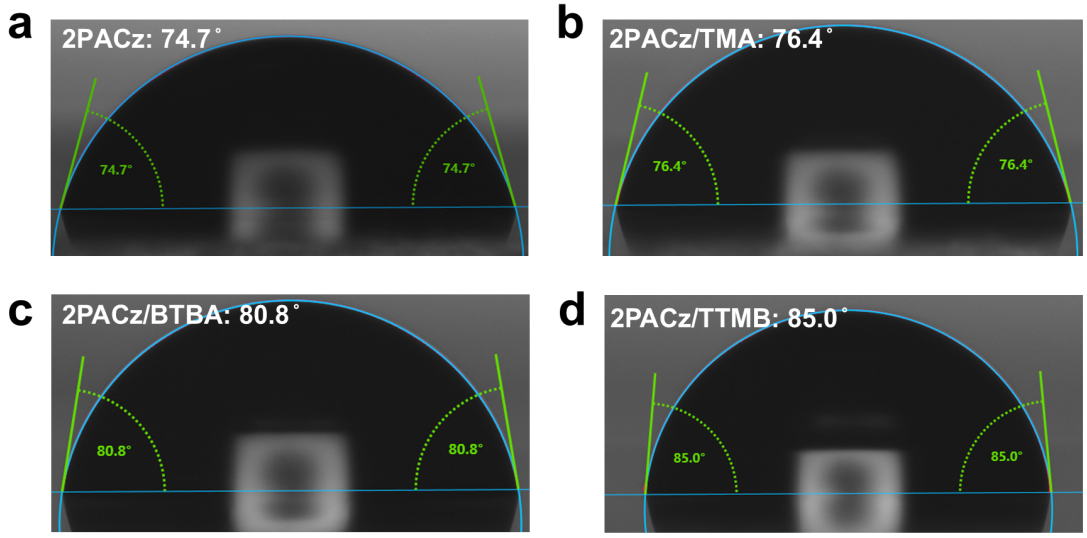

Supplementary Fig. 2. Contact angle measurements of perovskite precursor droplet on SAM/ITO/glass substrates prepared from 2PACz solutions with different additives. (**a**) pristine 2PACz without additive, (**b**) 2PACz with TMA, (**c**) 2PACz with BTBA, and (**d**) 2PACz with TTMB.

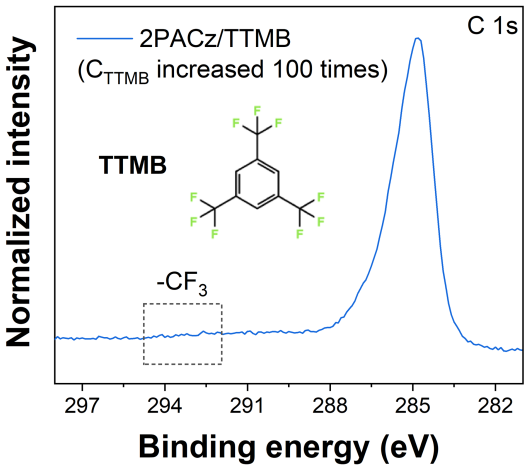

Supplementary Fig. 3. C 1s XPS spectrum of SAM/ITO/glass sample prepared from a 0.4 mg/mL 2PACz solution containing TTMB at a molar ratio of TTMB:2PACz =100:4.

To evaluate whether TTMB can adsorb on the ITO substrate during SAM deposition, we increased the TTMB concentration in the 2PACz/TTMB system from a molar ratio of 1:4 to 100:4. Even at this two-orders-of-magnitude higher concentration, the XPS spectrum (Supplementary Fig. 3) shows no detectable -CF_3 signal, confirming that TTMB does not anchor on the ITO surface during the SAM deposition process.

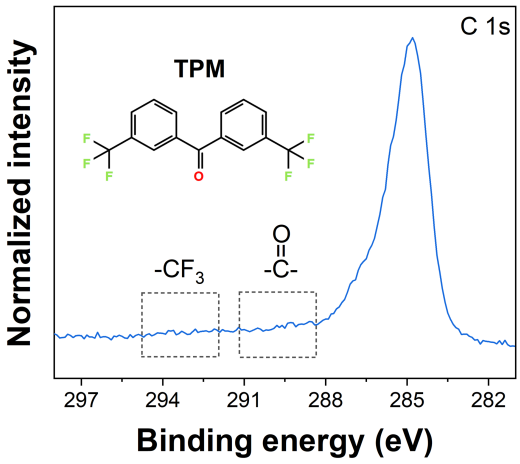

Supplementary Fig. 4. C 1s XPS spectrum of SAM/ITO/glass sample prepared from a 0.4 mg/mL 2PACz solution containing bis[3-(trifluoromethyl)phenyl]methanone (TPM) additive at a molar ratio of TPM:2PACz = 1:4.

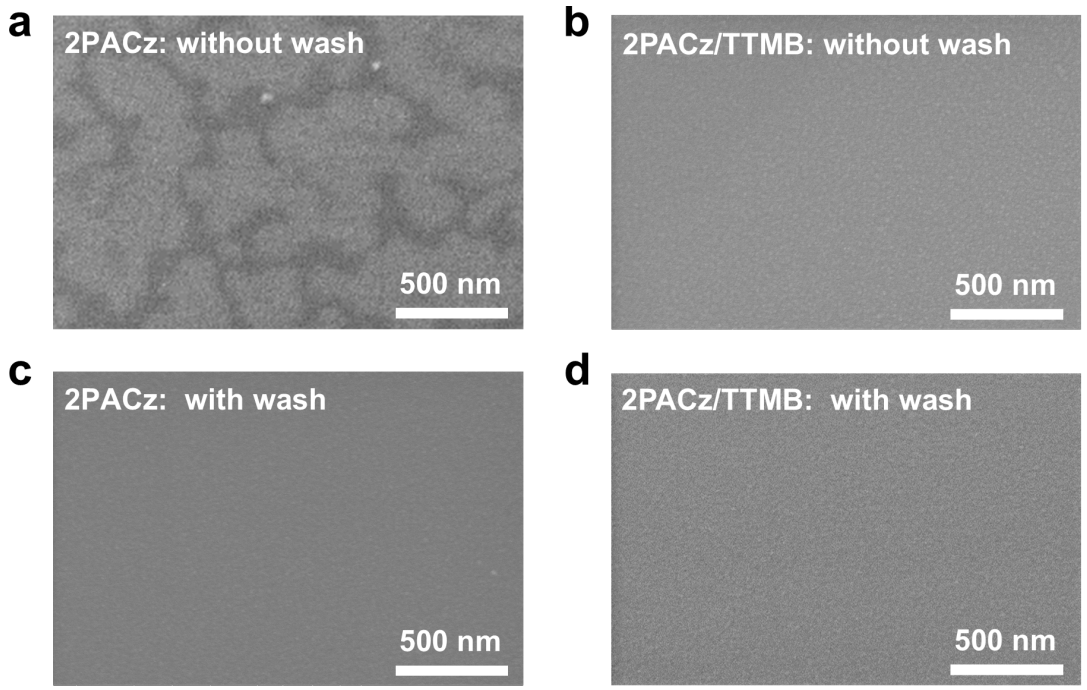

Supplementary Fig. 5. SEM images of SAM films on flat ITO/silicon substrates prepared from 2PACz solutions without and with TTMB, before and after the washing step. (**a**) pristine 2PACz solution (0.4 mg/mL) spin-coated at 3000 rpm for 30 s and annealed without washing. (**b**) 2PACz/TTMB solution (0.4 mg/mL 2PACz with 25 mol% TTMB relative to 2PACz) spin-coated at 3000 rpm for 30 s and annealed without washing. (**c**) pristine 2PACz solution spin-coated, annealed, washed, and re-annealed; (**d**) 2PACz/TTMB solution spin-coated, annealed, washed, and re-annealed.

To examine whether 2PACz micellar aggregates deposit on the ITO substrate during SAM formation, ITO-coated flat silicon substrates were used to minimize morphological artifacts arising from substrate roughness. For SAM prepared from pristine 2PACz solution (0.4 mg/mL), SEM image of unwashed sample (Supplementary Fig. 5a) reveals non-uniform deposition with pronounced aggregated features. After

standard washing (Supplementary Fig. 5c), these aggregates are removed, yielding a more uniform 2PACz distribution, which indicates that even if aggregates initially deposit on the ITO, they are weakly adsorbed and can be removed during washing. In contrast, for the 2PACz/TTMB system, no aggregates are observed either before or after washing (Supplementary Figs. 5b and 5d), demonstrating that TTMB effectively suppresses aggregation during SAM deposition.

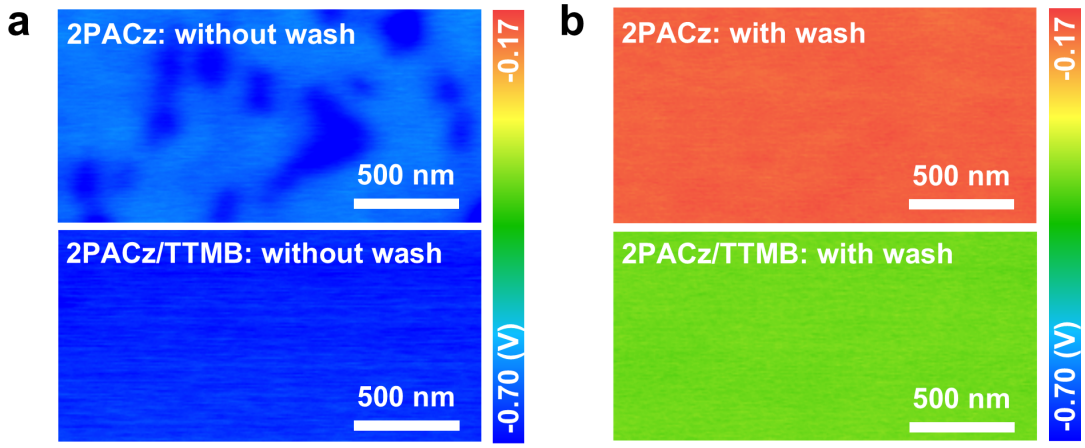

Supplementary Fig. 6. KPFM images of SAM films on flat ITO/silicon substrates (a) without and (b) with the washing step. before and after the washing step.

KPFM of unwashed pristine 2PACz films on flat ITO/silicon revealed pronounced aggregates and local surface-potential depressions, which were removed after washing, indicating weak adsorption of aggregates (Supplementary Fig. 6a). In contrast, 2PACz/TTMB films exhibited no aggregates before or after washing, with spatially uniform surface potentials and more negative values, consistent with higher SAM coverage (Supplementary Fig. 6b).

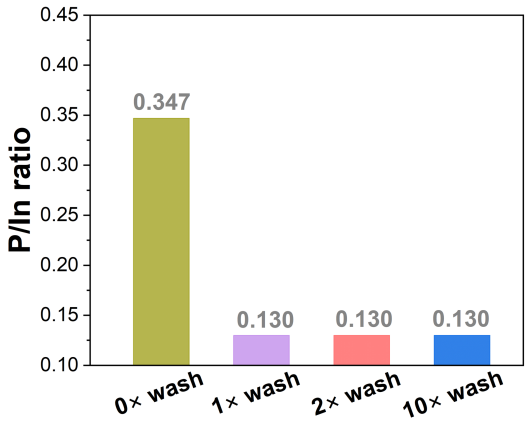

Supplementary Fig. 7. P/In XPS atomic ratios of SAM/ITO/glass samples prepared from a 0.4 mg/mL 2PACz solution without washing and with multiple wash cycles.

The effect of the washing process on the P/In ratio was investigated. For SAM/ITO/glass samples prepared from a 0.4 mg/mL 2PACz solution without washing, the P/In ratio is 0.347 (Supplementary Figs. 7-8). After a single washing cycle, the P/In ratio decreases significantly to 0.130, reflecting the removal of unbonded 2PACz species. Notably, the P/In ratio remains constant at 0.130 even after ten consecutive washing cycles, indicating that solvent washing selectively removes unbonded molecules while the bonded 2PACz remains stably attached to the ITO substrate.

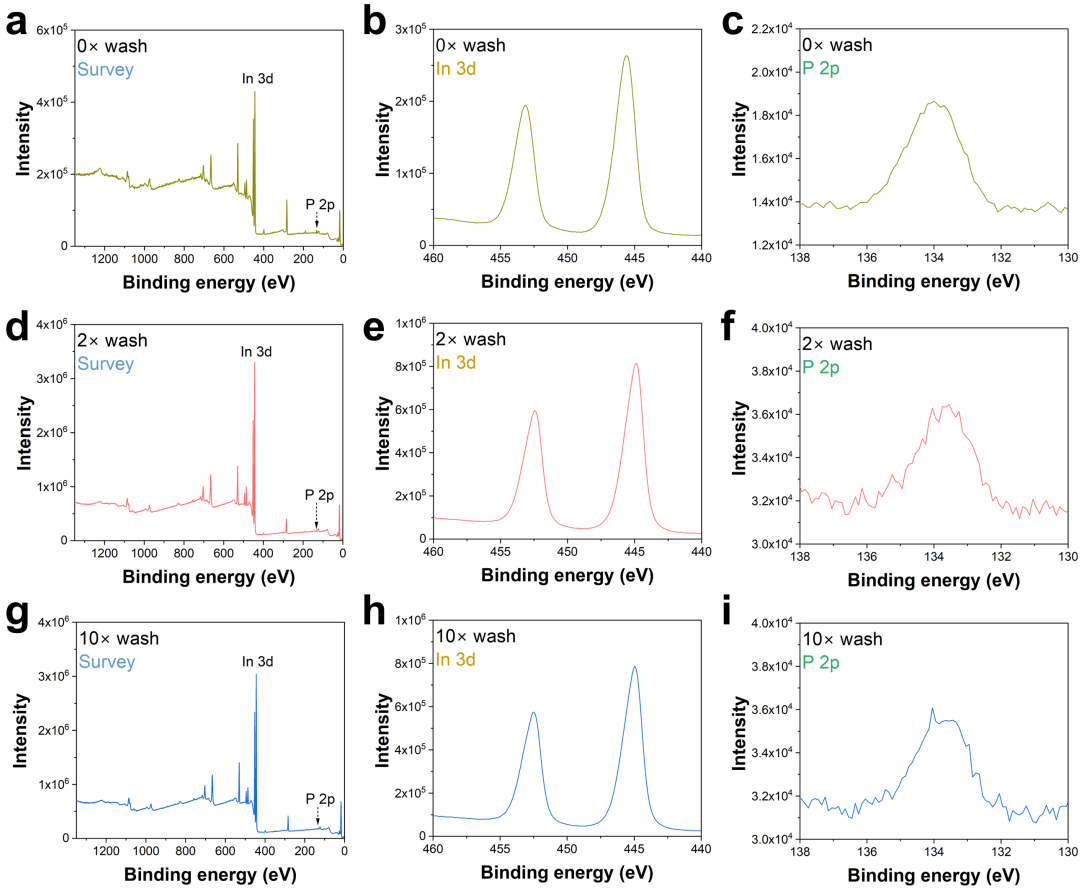

Supplementary Fig. 8. XPS spectra of SAM/ITO/glass samples prepared from a 0.4 mg/mL 2PACz solution. (**a-c**) 2PACz deposition without wash step. (**d-f**) with 2 wash steps. (**g-i**) with 10 wash steps. (**a, d, g**) XPS survey spectra. (**b, e, h**) In 3d XPS spectra. (**c, f, i**) P 2p XPS spectra.

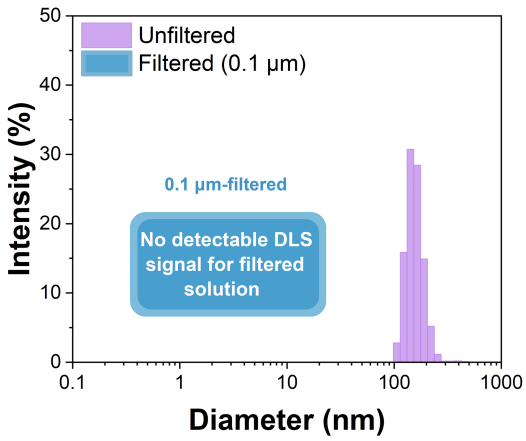

Supplementary Fig. 9. DLS measurements of unfiltered and 0.1 μm-filtered 2PACz solutions, showing no detectable scattering signal after filtration.

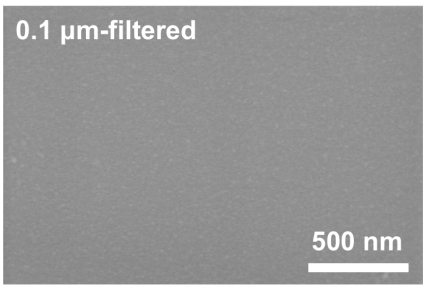

Supplementary Fig. 10. SEM image of 2PACz on flat ITO/silicon substrates prepared from 0.4 mg/mL 2PACz solution filtered by 0.1 μm PTFE filter.

The SEM image of a 2PACz film prepared from a 0.4 mg/mL solution filtered through a 0.1 μm PTFE membrane (Supplementary Fig. 10) shows a uniform surface without aggregates, in contrast to the pronounced aggregation observed for films deposited from unfiltered 2PACz solution (Supplementary Fig. 5a), confirming that filtration effectively removes micellar species in 2PACz solution.

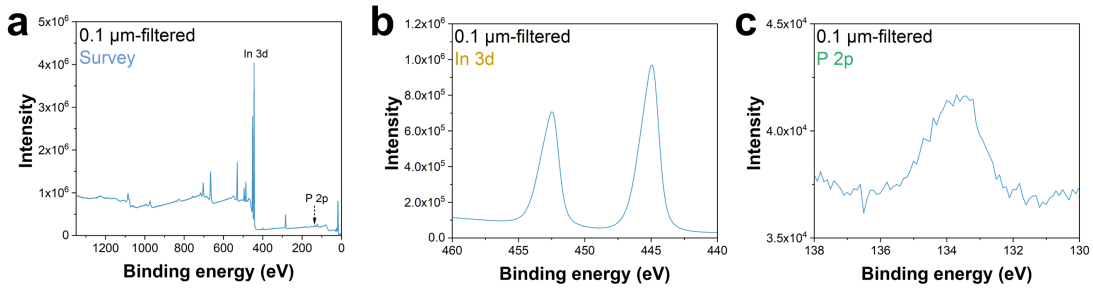

Supplementary Fig. 11. 2PACz/ITO/glass sample prepared from a 0.4 mg/mL 2PACz solution filtered through a 0.1 μm PTFE filter. (**a**) XPS survey spectrum, (**b**) In 3d XPS spectrum, and (**c**) P 2p XPS spectrum.

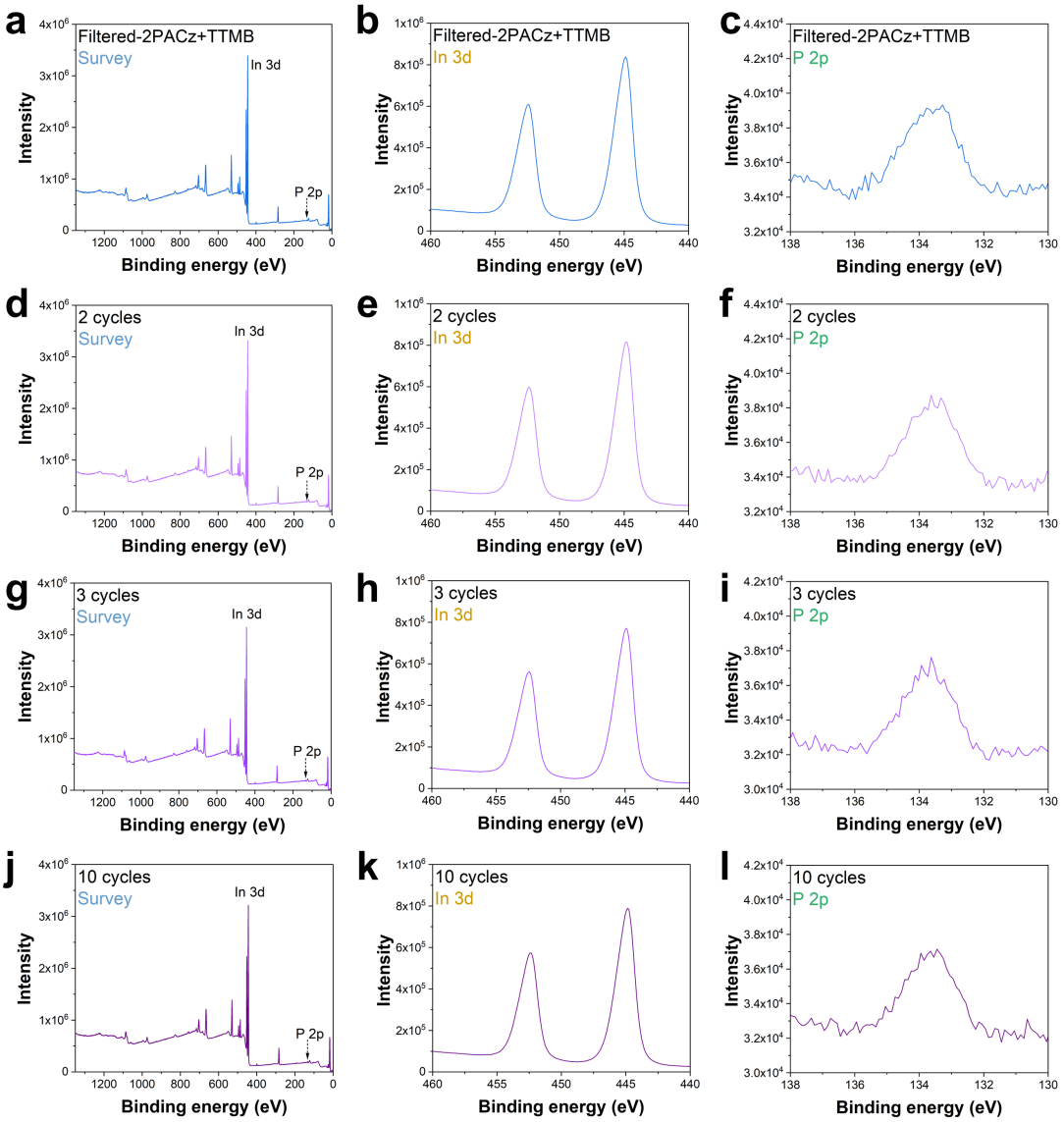

Supplementary Fig. 12. XPS spectra of SAM/ITO/glass samples prepared from a 0.4 mg/mL 2PACz solution filtered through a 0.1 μm PTFE filter using different spin-anneal-wash-reanneal cycles. (**a-c**) single cycle using filtered 2PACz with TTMB added after filtration (filtered-2PACz+TTMB). (**d-f**) 2 cycles. (**g-i**) 3 cycles. (**j-l**) 10 cycles. (**a, d, g, j**) XPS survey spectra. (**b, e, h, k**) In 3d XPS spectra. (**c, f, i, l**) P 2p XPS spectra.

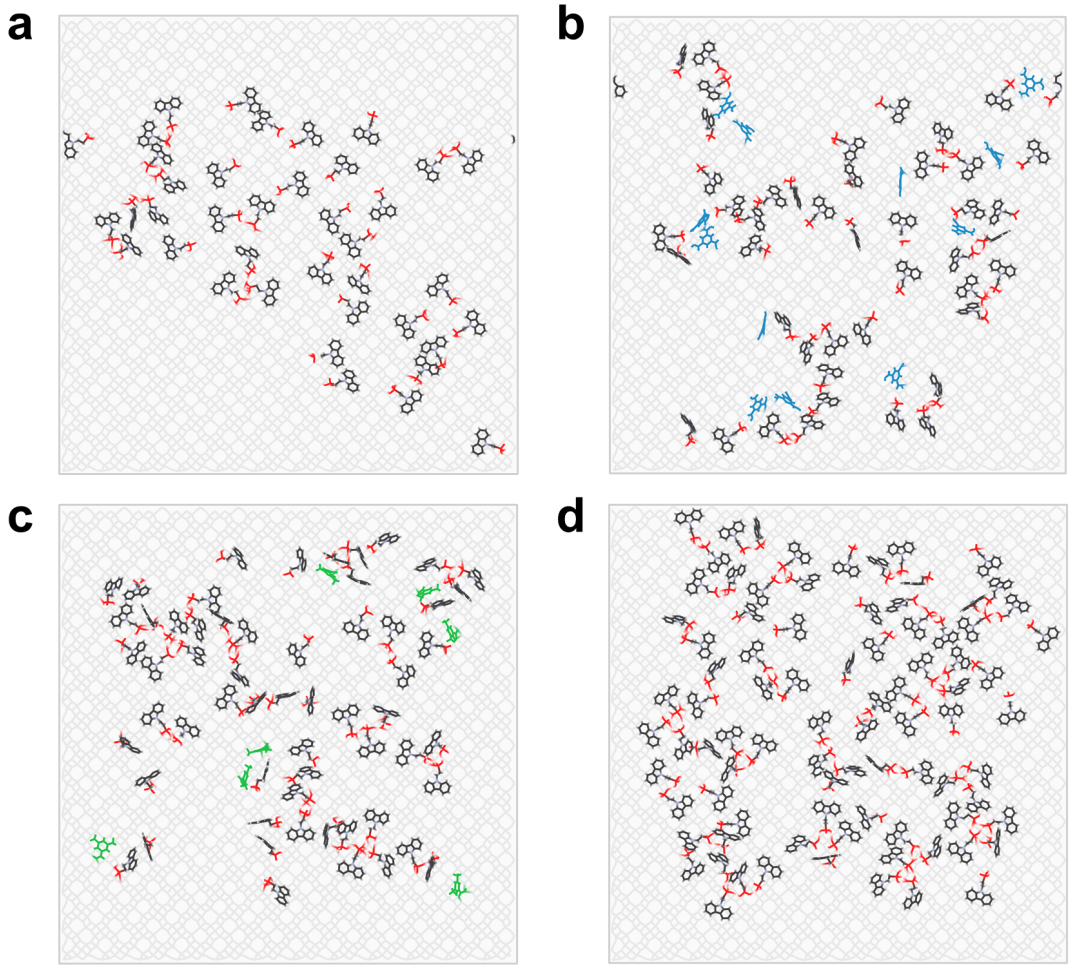

Supplementary Fig. 13. Top-view MD simulation results of anchored 2PACz molecules and anchored additives after removal of unbonded species for (**a**) pristine 2PACz, (**b**) 2PACz/TMA, (**c**) 2PACz/BTBA, and (**d**) 2PACz/TTMB.

Simulations were initiated with 300 randomly distributed 2PACz molecules, with or without 75 additive molecules, placed 10 Å above an ITO surface. After 5 ns of equilibration (Fig. 2a), unbonded species were removed to highlight the effective surface coverage of anchored 2PACz and additives. The top-view results are shown in Supplementary Fig. 13, with corresponding cross-sectional views in Fig. 2b. Bonding was determined using a Python code, where a 2PACz molecule was considered

anchored if any of its oxygen atoms were within 2.46 Å of an In atom on the ITO surface; all unbonded 2PACz molecules were removed. For additives, an additive molecule was retained if any of its oxygen atoms were within 2.46 Å of an In atom on ITO, or any fluorine atoms were within 2.05 Å of an In atom or with 1.42 Å of an O atom on ITO; otherwise, it was removed.

After this procedure, the number of anchored molecules for each system was: pristine 2PACz, 39 molecules; 2PACz/TMA, 45 2PACz molecules and 12 TMA molecules; 2PACz/BTBA, 59 2PACz molecules and 7 BTBA molecules; 2PACz/TTMB, 86 2PACz molecules and 0 TTMB molecules.

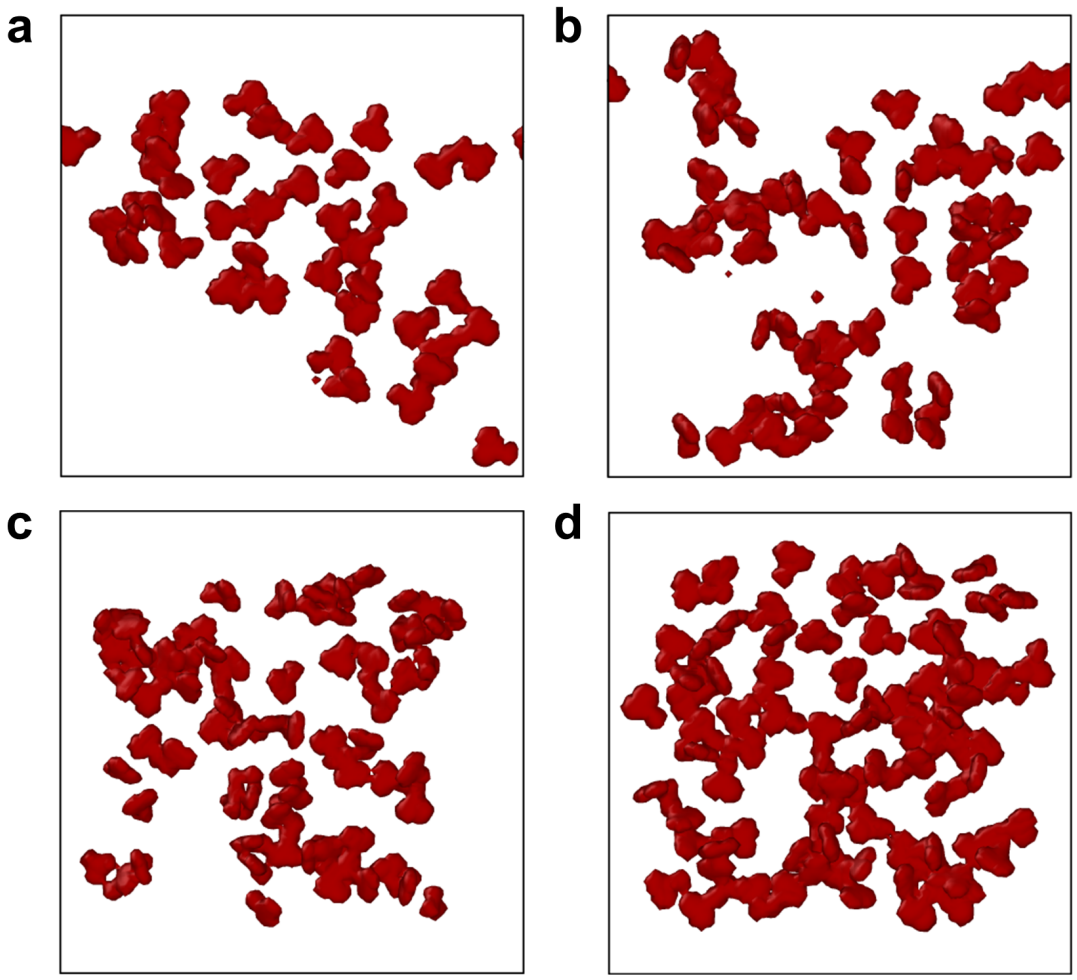

Supplementary Fig. 14. Surface coverage calculation models derived from top-view MD simulation results after removal of unanchored species (based on Supplementary Fig. 13) for (**a**) pristine 2PACz, (**b**) 2PACz/TMA, (**c**) 2PACz/BTBA, and (**d**) 2PACz/TTMB.

The overall surface coverage of bonded 2PACz and bonded additive molecules on the ITO substrate was quantified using the Construct Surface Mesh function in OVITO, applying the Gaussian density method (Resolution: 100; Radius scaling: 100%; Iso value: 0.2). This approach provides a quantitative evaluation of molecular packing

density and surface coverage. The calculated surface coverage values for each 2PACz system are summarized in Fig. 2c.

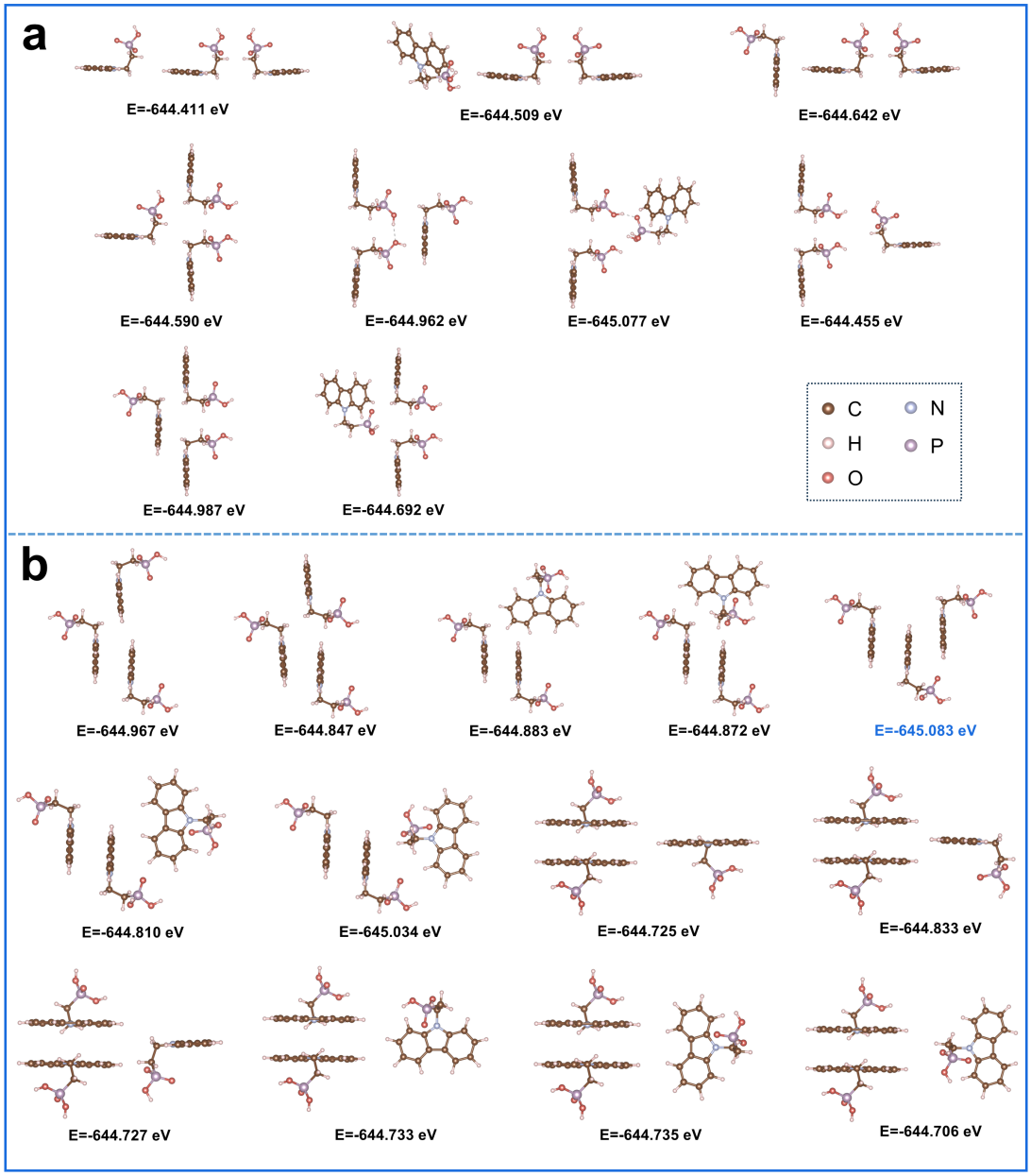

Supplementary Fig. 15. Energy model of 2PACz under different stacking configurations. Two stacking scenarios were considered. (**a**) third-molecule insertion based on phosphate-group stacking and (**b**) third-molecule insertion based on carbazole-group stacking.

Energy analysis in Supplementary Fig. 15 indicates that the carbazole-stacked

configuration with third-molecule insertion represents the minimum-energy state of 2PACz. The lowest-energy structure is highlighted in blue in Supplementary Fig. 15, with an energy of -645.083 eV. This structure was subsequently used for all further calculations of the intermolecular binding energy of 2PACz.

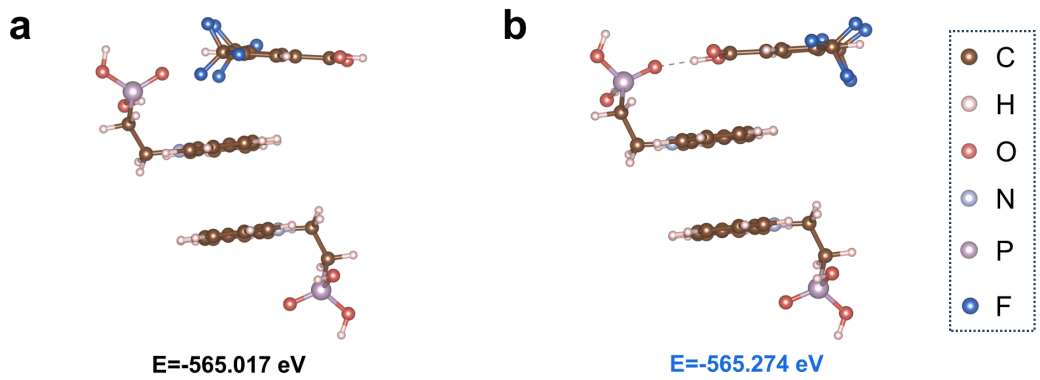

Supplementary Fig. 16. Lowest-energy model of 2PACz/BTBA. The minimum-energy 2PACz stacking model from Supplementary Fig. 15 was used, with the -COOH group of BTBA oriented in two different directions: (**a**) outward and (**b**) inward.

The result in Supplementary Fig. 16 indicate that the inward-oriented -COOH configuration corresponds to the overall minimum-energy state for 2PACz/BTBA system. Therefore, the inward-oriented configuration was used for all subsequent calculations of the 2PACz/BTBA system.

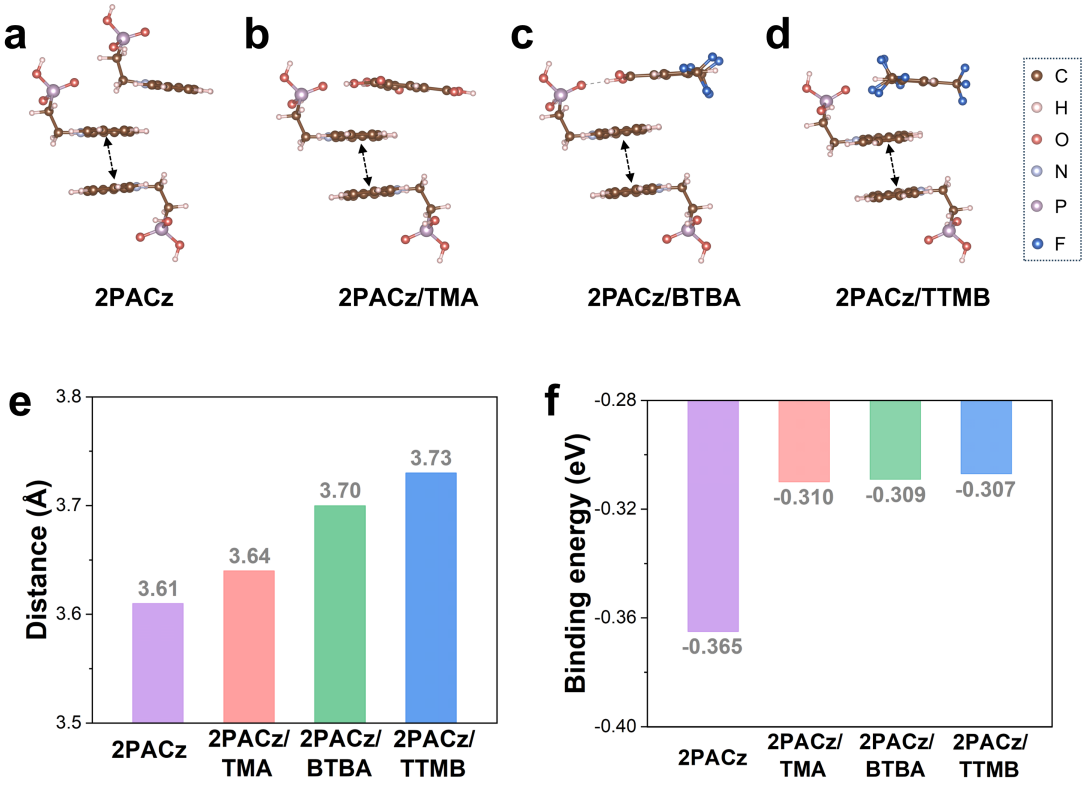

Supplementary Fig. 17. (a-d) Binding energy models of 2PACz with different additives: (**a**) pristine 2PACz without additive, (**b**) 2PACz with TMA, (**c**) 2PACz with BTBA (using the inward-oriented -COOH configuration from fig. S16b), and (**d**) 2PACz with TTMB. (**e**) Calculated intermolecular distance and (**f**) calculated intermolecular binding energy of 2PACz molecules in the absence and presence of TMA, BTBA, or TTMB.

The intermolecular binding energy models of 2PACz with different additives are shown in Supplementary Figs. 17a-17d. The calculated intermolecular distances and binding energies of 2PACz molecules, in the absence and presence of TMA, BTBA, or TTMB, are presented in Supplementary Figs. 17e and 17f, respectively. The results indicate that TTMB incorporation reduces the intermolecular interactions between 2PACz molecules, effectively promoting their dispersion.

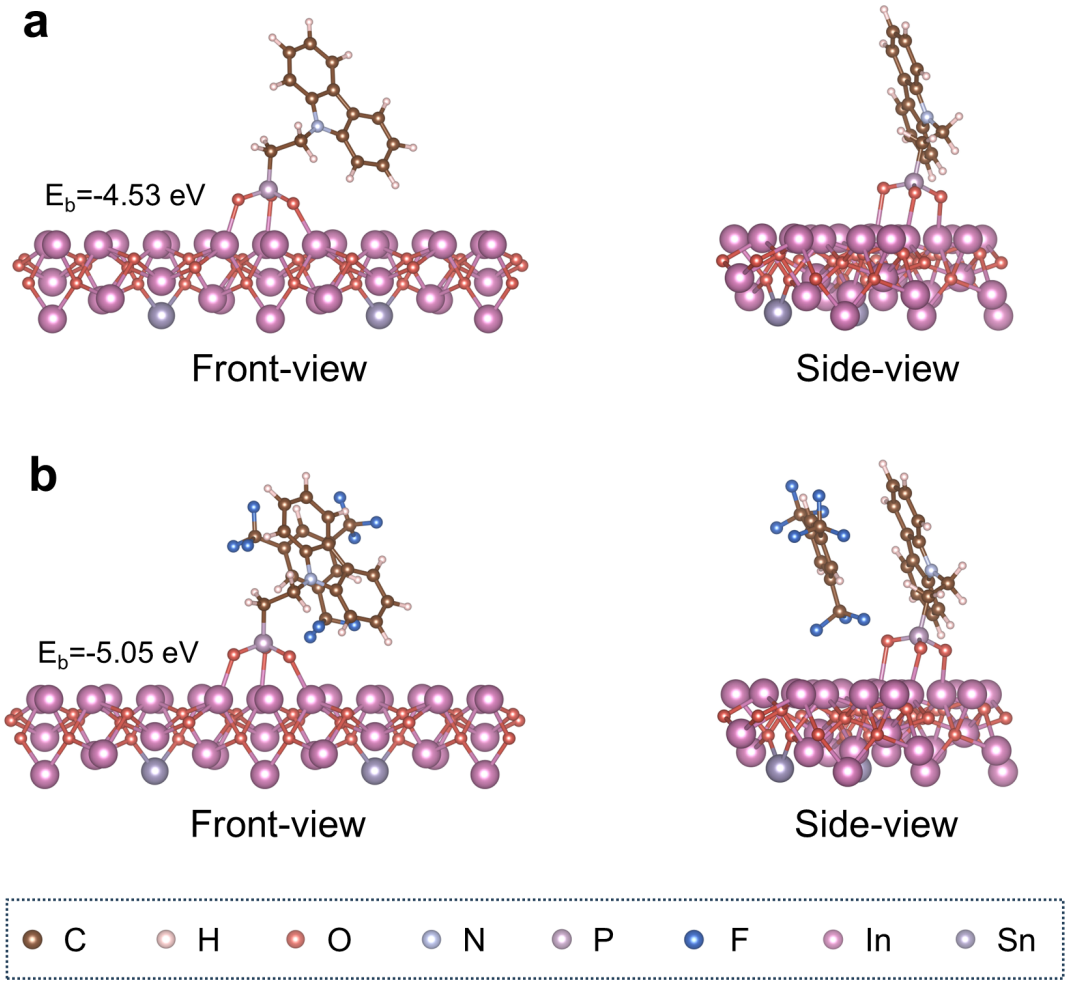

Supplementary Fig. 18. Binding energy model of 2PACz on the ITO substrate for (**a**) pristine 2PACz and (**b**) 2PACz/TTMB.

The binding energy of 2PACz on ITO increases from -4.53 eV to -5.05 eV in the presence of TTMB (Supplementary Fig. 18), indicating that TTMB enhances the interfacial anchoring of individual 2PACz molecule on ITO substrate.

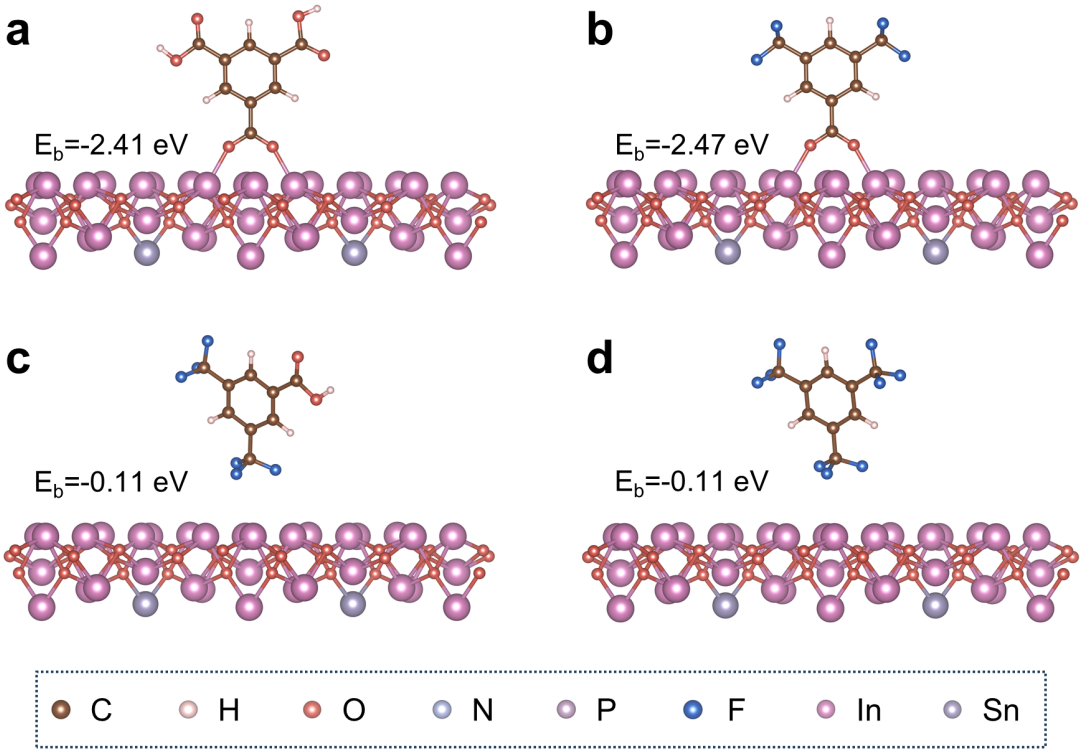

Supplementary Fig. 19. Adsorption energy models of different additive molecules on the ITO substrate. (**a**) TMA, (**b**) BTBA binding via the -COOH group, (**c**) BTBA binding via the $-CF_3$ group, and (**d**) TTMB.

Adsorption-energy calculations in Supplementary Fig. 19 indicate that the $-CF_3$ groups in TTMB interact only weakly with ITO (around -0.1 eV), whereas the -COOH groups in TMA and BTBA bind strongly, with energies of -2.41 eV and -2.47 eV, respectively.

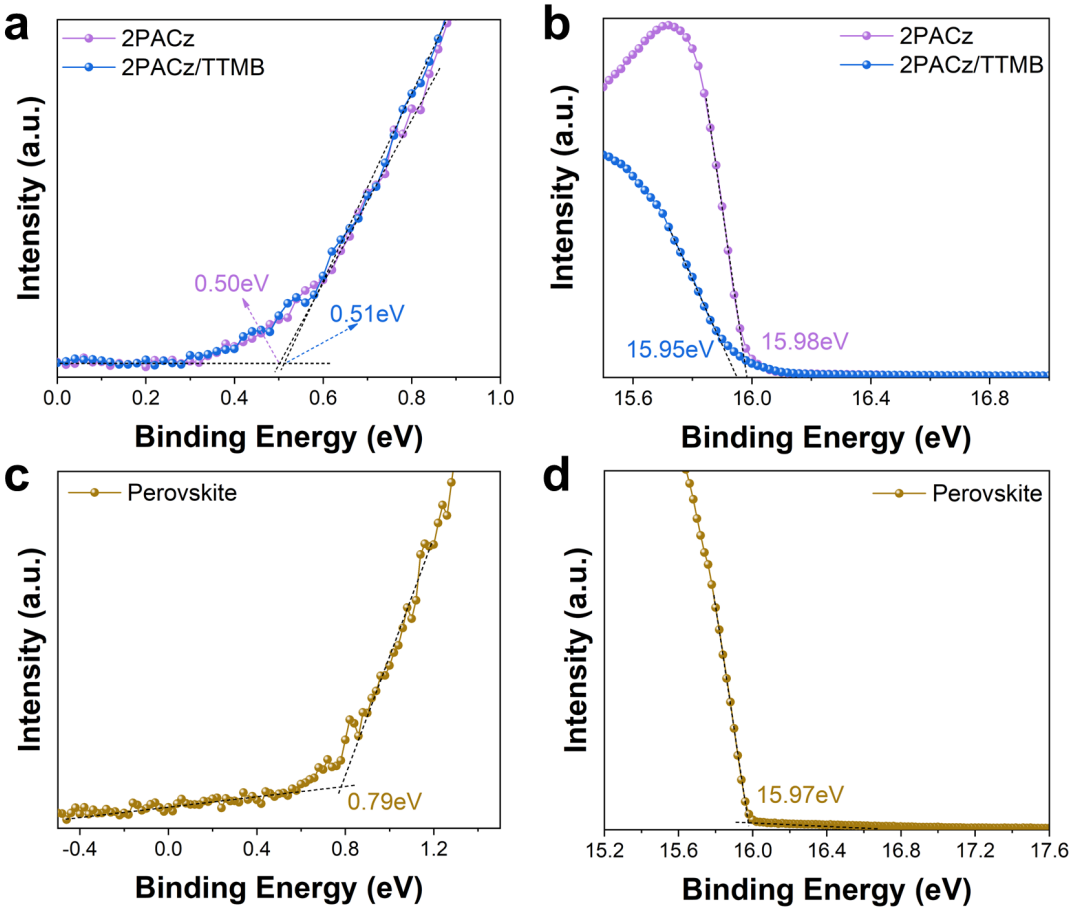

Supplementary Fig. 20. Ultraviolet photoelectron spectroscopy (UPS) measurement for 2PACz and 2PACz/TTMB on ITO glass substrate: (**a**) valence band onset region of UPS spectra, and (**b**) secondary electron cutoff region of UPS spectra. UPS measurement for perovskite film on 2PACz/ITO/glass substrate: (**c**) valence band onset region of UPS spectrum, and (**d**) secondary electron cutoff region of UPS spectrum.

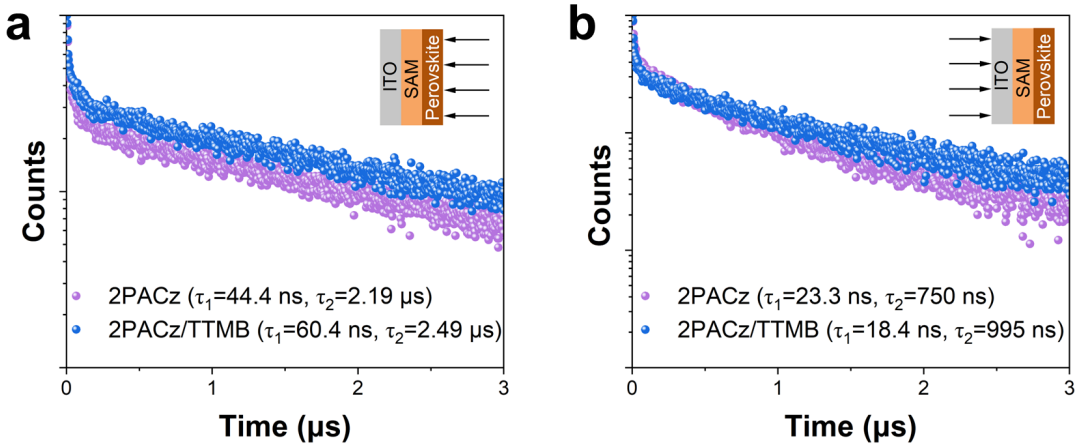

Supplementary Fig. 21. TRPL measurements of perovskite films on SAM/ITO/glass substrates based on pristine 2PACz and 2PACz/TTMB, with excitation from (**a**) the perovskite side and (**b**) the ITO side.

The TRPL decay curves of perovskite samples were fitted using a biexponential function:

$$Y(t) = A+B_1\exp(-t/\tau_1) + B_2\exp(-t/\tau_2)$$

where τ_1 and τ_2 are the fast and slow decay time constants, respectively, and A, B_1 and B_2 are the corresponding amplitudes, representing the relative contributions of each decay component to the normalized signal.

For excitation from the perovskite side (Supplementary Fig. 21a), the slow decay component τ_2 increased from 2.19 μs for perovskite film on pristine 2PACz to 2.49 μs on 2PACz/TTMB, indicating improved perovskite film quality. In contrast, for excitation from the ITO side (Supplementary Fig. 21b), the fast decay component τ_1 decreased from 23.3 ns for perovskite film on pristine 2PACz to 18.4 ns on

2PACz/TTMB, suggesting that SAM deposited with TTMB facilitates interfacial charge transport.

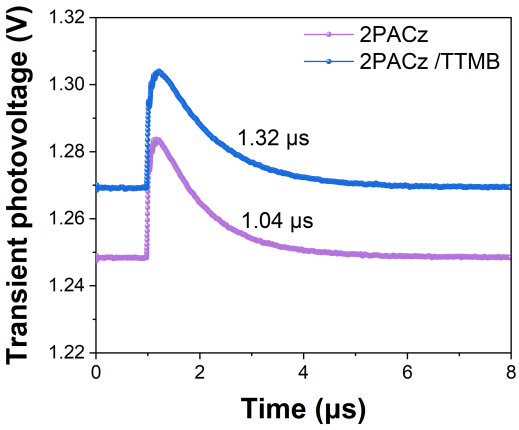

Supplementary Fig. 22. Transient photovoltage (TPV) decay curves for perovskite solar cells based on pristine 2PACz and 2PACz/TTMB.

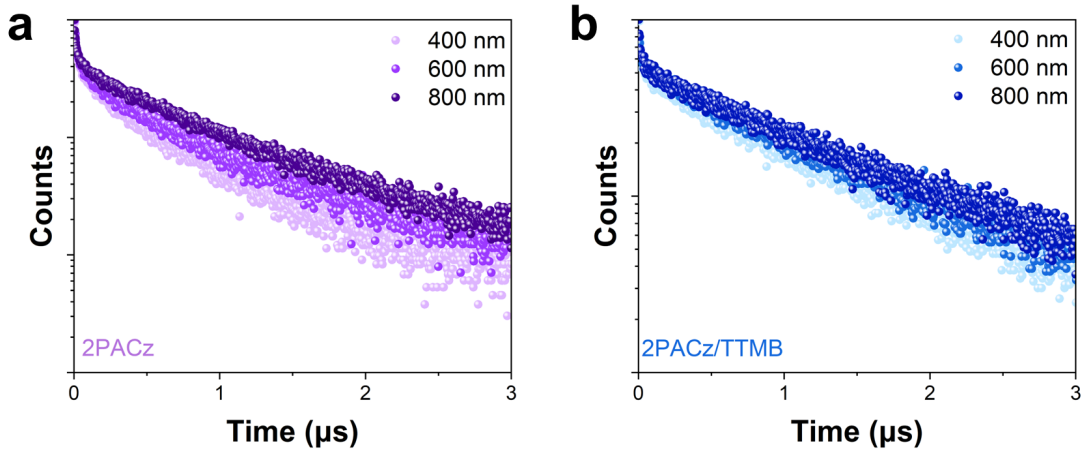

Supplementary Fig. 23. TRPL measurements of perovskite films on SAM/ITO/glass substrates with varying perovskite thicknesses (400, 600, and 800 nm), excited from the ITO side. (**a**) pristine 2PACz and (**b**) 2PACz/TTMB.

Perovskite films of varying thickness were deposited on SAM/ITO/glass substrates prepared with either pristine 2PACz or 2PACz/TTMB. Using carrier lifetimes obtained from TRPL measurements (Supplementary Fig. 23) and their dependence on film thickness, the bulk carrier lifetime (τ_b) and surface recombination velocity (SRV) were estimated via a double-heterostructure model [1-3], with the fitting results shown in Fig. 3g.

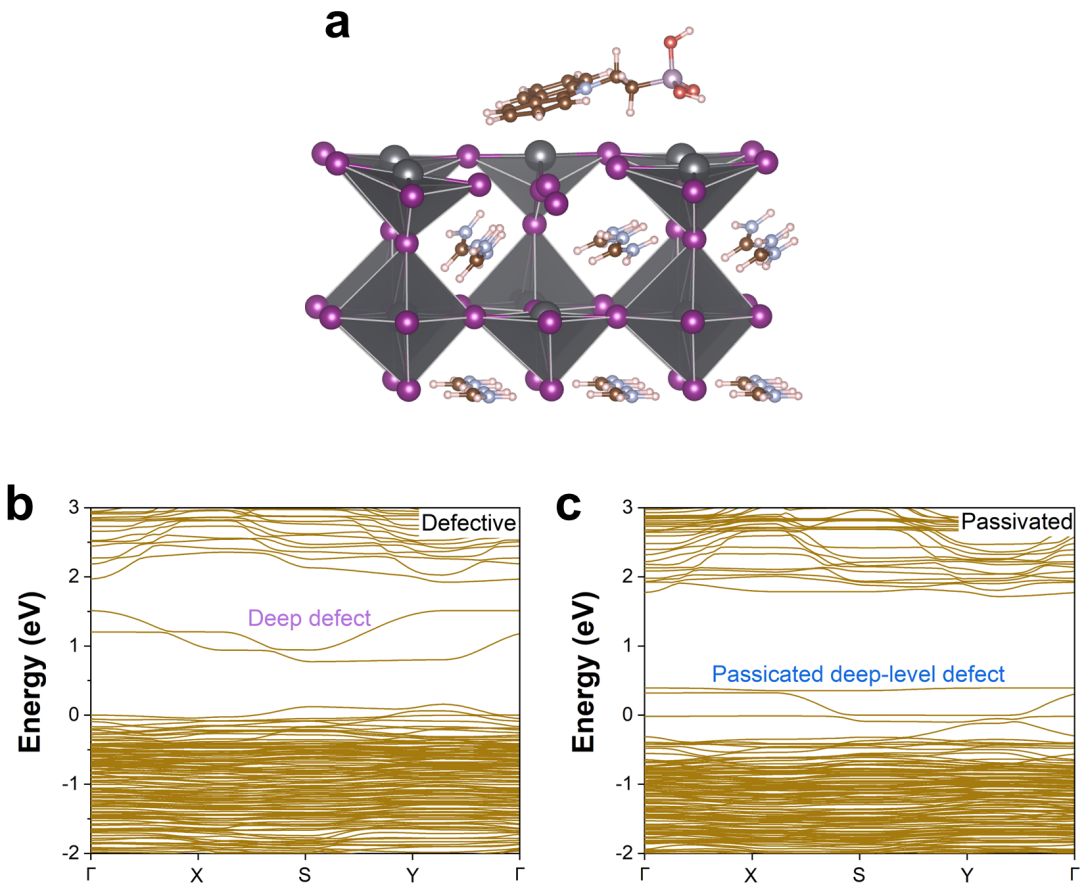

Supplementary Fig. 24. (**a**) DFT optimized structure of a perovskite surface passivated by 2PACz. (**b, c**) Simulations of the V_{Pb}^{2+} defective perovskite passivated by 2PACz. (b) calculated density of states of perovskite with V_{Pb}^{2+} defects, (c) calculated density of states of perovskite with V_{Pb}^{2+} defects passivated by carbazole functional groups of 2PACz.

DFT calculations were carried out to investigate the passivation of Pb-vacancy defects (V_{Pb}^{2+}) in perovskite by 2PACz, following the procedure reported[4], with the detailed structural model shown in Supplementary Fig. 24a. Dipole corrections were applied along the z-direction, and slab relaxations were performed at the Γ point with the bottom layers fixed. Electronic structure calculations employed a 2 × 2 × 1 Γ-

centered k-mesh, and the band structures were computed using 40 k-points in the two-dimensional Brillouin zone. The results in Supplementary Fig. 24 indicate that the carbazole groups in 2PACz effectively passivate deep-level Pb-vacancy defects.

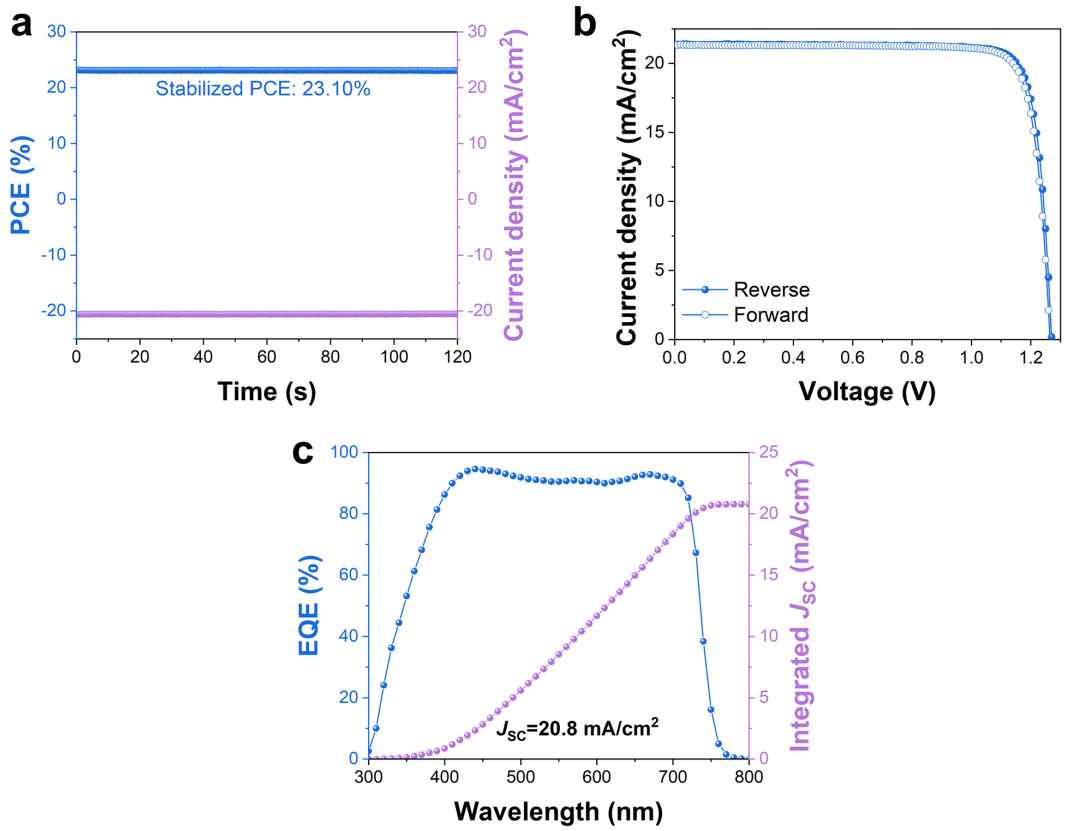

Supplementary Fig. 25. (**a**) Stabilized power output, (**b**) reverse and forward *J-V* scans, (**c**) EQE and integrated J_{SC} of single-junction perovskite solar cell based on 2PACz/TTMB.

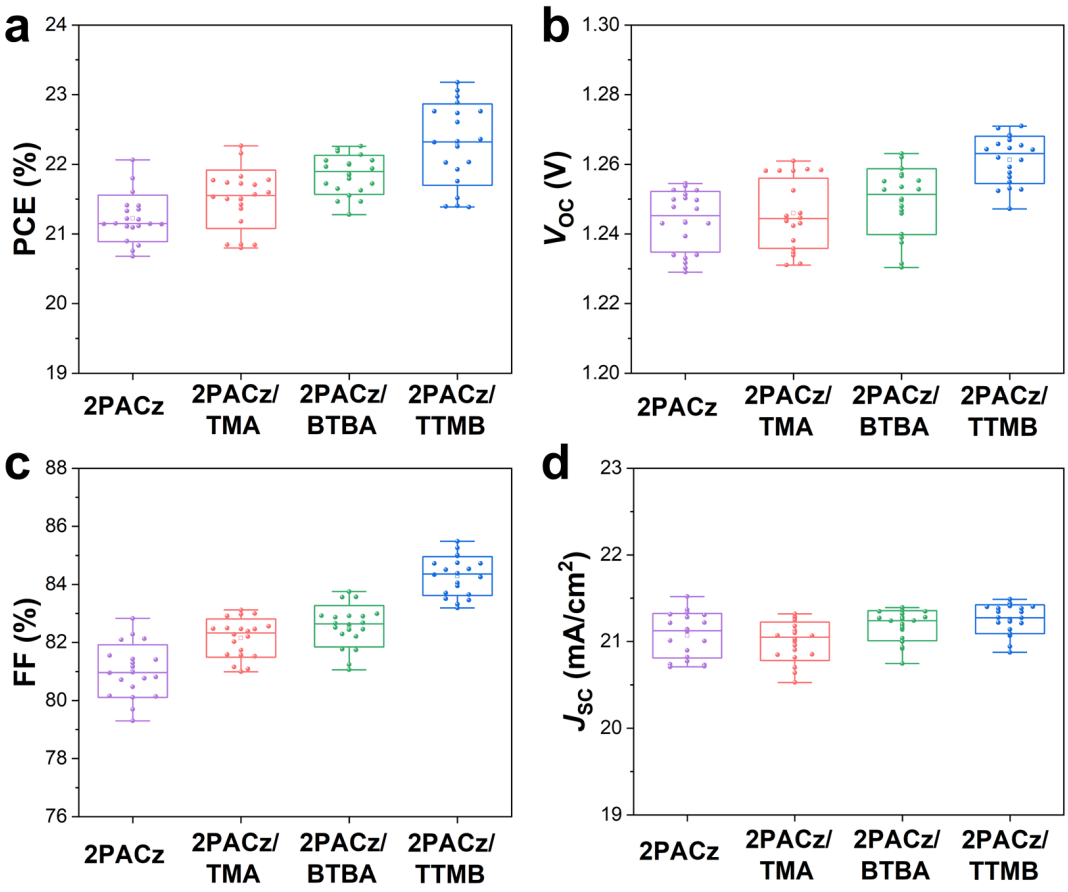

Supplementary Fig. 26. Statistics of photovoltaic parameters of single-junction solar cells based on pristine 2PACz and 2PACz with different additives. (**a**) PCE, (**b**) V_{OC}, (**c**) FF, and (**d**) J_{SC}. Box plot represents the standard deviation, the central line shows the median, and the white square represents the mean value.

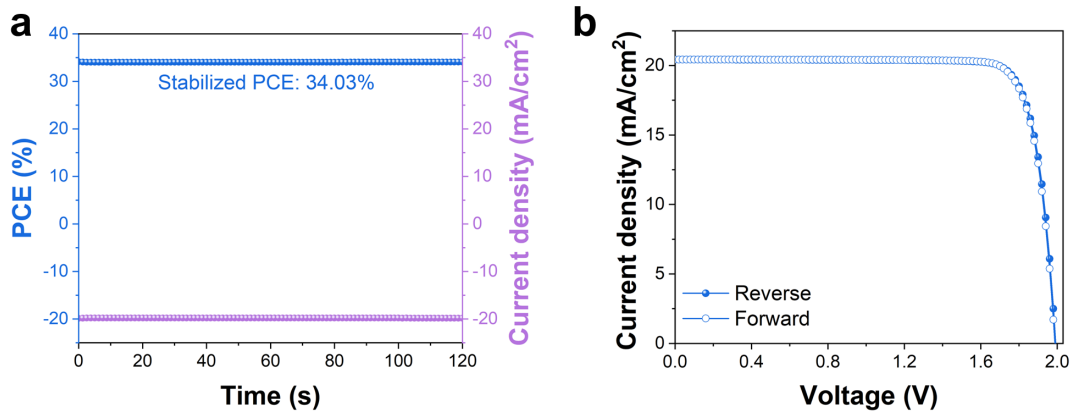

Supplementary Fig. 27. (**a**) Stabilized power output and (**b**) reverse and forward *J-V* scans of perovskite/Si tandem solar cell based on 2PACz/TTMB.

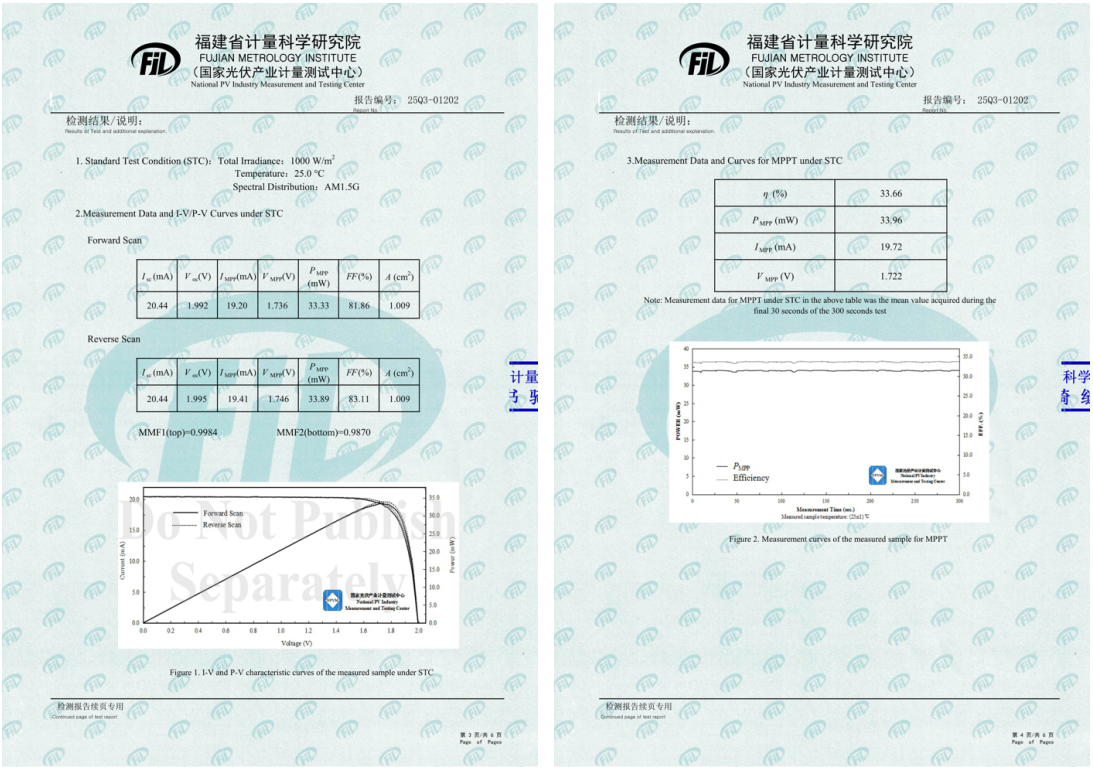

Supplementary Fig. 28. Certification report of the perovskite/silicon tandem solar cell measured at the Fujian Institute of Metrology, China. The report includes detailed photovoltaic parameters, forward and reverse *I-V* curves, and steady-state power output.

Measurements were performed using a dual-light source solar simulator (xenon and halogen) at the Fujian Institute of Metrology, China, calibrated using the measured EQE and a certified reference silicon cell to achieve a spectral mismatch factor of 1.00 ± 0.02. The total irradiance was set to 1000 W/m^2 based on the short-circuit current of the reference solar cell. The certified stabilized power outut of perovskite/silicon tandem solar cell is 33.66%.

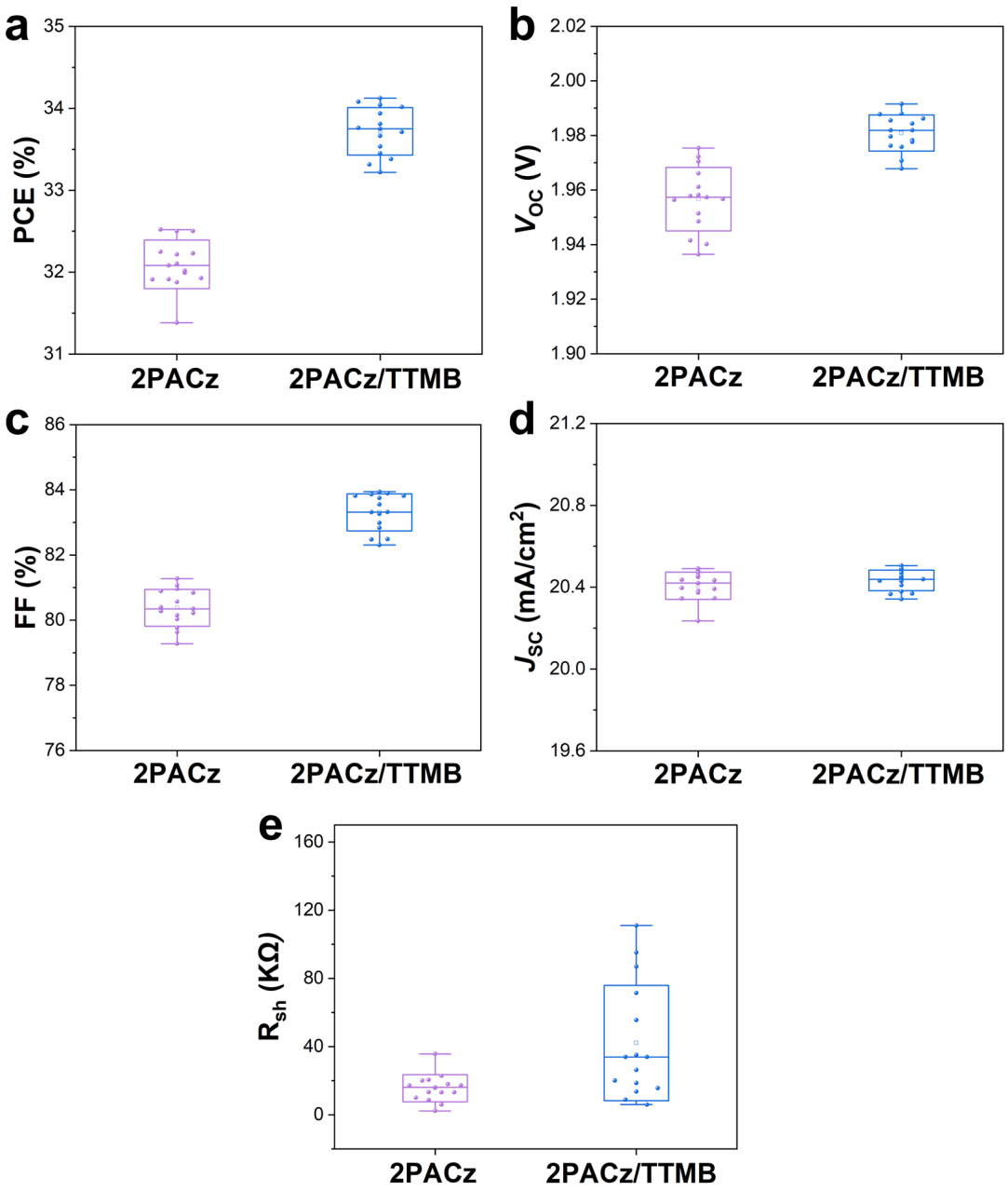

Supplementary Fig. 29. Statistics of photovoltaic parameters for perovskite/silicon tandem solar cells based on pristine 2PACz and 2PACz/TTMB. (**a**) PCE, (**b**) V_{OC}, (**c**) FF, (**d**) J_{SC}, and (**e**) R_{sh}. Box plot represents the standard deviation, the central line shows the median, and the white square represents the mean value.

Supplementary References

1. Peng, W. et al. Reducing nonradiative recombination in perovskite solar cells with a porous insulator contact. *Science* **379**, 683-690 (2023).
2. Tong, J. et al. Carrier control in Sn–Pb perovskites via 2D cation engineering for all-perovskite tandem solar cells with improved efficiency and stability. *Nat. Energy* **7**, 642-651 (2022).
3. Stranks, S. D. et al. Electron-hole diffusion lengths exceeding 1 micrometer in an organometal trihalide perovskite absorber. *Science* **342**, 341 (2013).
4. Liu, S. et al. Buried interface molecular hybrid for inverted perovskite solar cells. *Nature* **632**, 536-542 (2024).